Amino Acids (2015) 47:153–162
DOI 10.1007/s00726-014-1855-3

ORIGINAL ARTICLE

Ac-*t*Leu-Asp-H is the minimal and highly effective human caspase-3 inhibitor: biological and in silico studies

Anna Ferrucci · Loris Leboffe · Mariangela Agamennone · Antonella Di Pizio · Marco Fiocchetti · Maria Marino · Paolo Ascenzi · Grazia Luisi

Received: 31 March 2014 / Accepted: 9 October 2014 / Published online: 21 October 2014

Abstract Caspase-3 displays a pivotal role as an executioner of apoptosis, hydrolyzing several proteins including the nuclear enzyme poly(ADP-ribose)polymerase (PARP). Ac-Asp-Glu-Val-Asp-H ($K_i^\circ = 2.3 \times 10^{-10}$ M at pH 7.5 and 25.0 °C), designed on the basis of the cleavage site of PARP, has been reported as a highly specific human caspase-3 inhibitor. Here, di- and tri-peptidyl aldehydes **11–13** and **27–29** have been synthesized to overcome the susceptibility to proteolysis, the intrinsic instability, and the scarce membrane permeability of the current inhibitors. Compounds **11–13**, **27–29** inhibit in vitro human caspase-3 competitively, values of K_i° ranging between 6.5 ($\pm$0.82) $\times 10^{-9}$ M and 1.1 ($\pm$0.04) $\times 10^{-7}$ M (at pH 7.4 and 25.0 °C). Moreover, the most effective caspase-3 inhibitor **11** impairs apoptosis in human DLD-1 colon adenocarcinoma cells. Furthermore, the binding mode of **11–13** and **27–29** to human caspase-3 has been investigated in silico. The comparative analysis of human caspase-3 inhibitors indicates that (1) aldehyde **11** is the minimal highly effective inhibitor, (2) the *t*Leu-Asp sequence is pivotal for satisfactory enzyme inhibition, and (3) the occurrence of the *t*Leu residue at the inhibitor P2 position is fundamental for enzyme/inhibitor recognition. Moreover, calculations suggest that the *t*Leu residue reduces the conformational flexibility of the inhibitor that binds to the enzyme with a lower energetic penalty.

Keywords Human caspase-3 · Peptidyl aldehyde inhibitors · Enzyme competitive inhibition · Human DLD-1 colon adenocarcinoma cells · Apoptosis · MM-GBSA

Abbreviations

AcOH	Acetic acid
AMC	7-Amino-4-methyl coumarin
DBU	1,8-Diazabicyclo [5.4.0] undec-7-ene
DCM	Dichloromethane
DMSO	Dimethylsulfoxide
DTT	Dithiothreitol
EDAC	*N*-ethyl-*N*′-(dimethylaminopropyl)-carbodiimide hydrochloride
E2	17β-Estradiol
ECL	Enhanced chemiluminescence
Fmoc	9-Fluorenylmethoxycarbonyl
Fomc	Phenoxymethylcarbonyl
HOBt	1-Hydroxybenzotriazole
MeOH	Methanol
NMM	*N*-methylmorfoline
O*t*Bu	*Tert*-butyl ester derivative
PAGE	Polyacrylamide gel electrophoresis
PARP	Poly(ADP-ribose)polymerase
RPMI	Roswell Park Memorial Institute
Sc	Semicarbazone derivative

A. Ferrucci and L. Leboffe contributed equally to this work.

Electronic supplementary material The online version of this article (doi:10.1007/s00726-014-1855-3) contains supplementary material, which is available to authorized users.

A. Ferrucci · M. Agamennone · G. Luisi (✉)
Department of Pharmacy, University "Gabriele d'Annunzio", Via dei Vestini 31, 66013 Chieti, Italy
e-mail: gluisi@unich.it

L. Leboffe · M. Fiocchetti · M. Marino · P. Ascenzi
Department of Sciences, University Roma Tre, Viale Guglielmo Marconi 446, 00146 Rome, Italy

A. Di Pizio
Institute of Biochemistry, Food Science and Nutrition, Robert H. Smith Faculty of Agriculture Food and Environment and Fritz Haber Center for Molecular Dynamics, The Hebrew University of Jerusalem, Herzl Street, P.O.B. 12, 76100 Rehovot, Israel

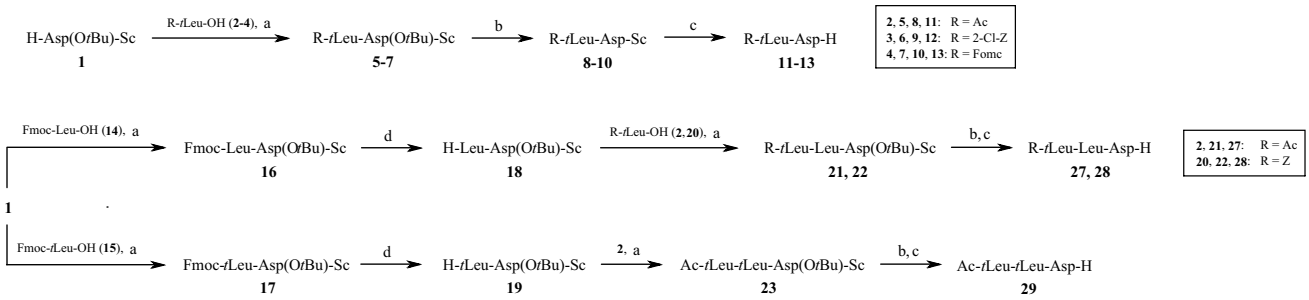

Fig. 1 Synthesis of peptidyl aldehydes **11–13** and **27–29**. Reagents and conditions: *a* EDAC, HOBt, NMM, DCM, 2 h at 0 °C, then overnight at room temperature; *b* 25 % TFA/DCM, 2 h at room temperature; *c* MeOH/AcOH/37 % HCHO (3:1:1), 3 h at room temperature; *d* DBU, DCM, 20 min at room temperature

TFA	Trifluoroacetic acid
*t*Leu	(S)-*tert*-leucine
Z	Benzyloxycarbonyl

Introduction

Apoptosis represents an evolutionarily conserved cell death program in eukaryotes, serving as a central function in cell differentiation and tissue plasticity (Bergmann and Steller 2010). A major role in regulation and execution of apoptotic events has been established for caspases, a family of structurally related intracellular proteases (Thornberry 1998; Chowdhury et al. 2008). It is well documented that misregulation of caspase-mediated apoptosis may result in aberrant cell demise or proliferation, finally leading to anomalies in tissue development and functions (Howley and Fearnhead 2008). In particular, an increased rate in caspase activity, mainly of the key executioner caspase-3, has been clearly related to either acute or chronic pathological conditions, such as ischemic stroke, myocardial infarction, and neurodegenerative diseases, and accordingly, the strategy of inhibiting this protease has been widely performed for therapeutic utility (Chatterjee et al. 2004; Ganesan et al. 2006; Kanthasamy et al. 2006; Rohn 2010).

Peptidyl inhibitors shorter than the canonical Asp-Glu-Val-Asp recognition sequence of the cleavage site of the nuclear enzyme poly(ADP-ribose)polymerase (PARP) have been reported to inhibit very efficiently human caspase-3, offering advantages in terms of solubility, cell permeability, and in vivo stability (Rotonda et al. 1996; Mittl et al. 1997; Talanian et al. 1997; Thornberry et al. 1997; Linton et al. 2002; Nedev et al. 2005). Based on this minimization approach, the Z-*t*Leu-Asp-H peptidyl inhibitor, displaying a very high affinity for caspase-3 ($K_i^\circ = 3.6\ (\pm 0.4) \times 10^{-9}$, at pH 7.4 and 25.0 °C) and a remarkable anti-apoptotic activity in vitro, was synthesized (Colantonio et al. 2008). This outcome was due to the unprecedented P2 positioning of the (*S*)-*tert*-leucine (*t*Leu) residue, which fits the S2 hydrophobic cavity of the enzyme with its bulky and highly lipophilic *tert*-butyl side chain. The removal of the P3 and P4 residues of the canonical Asp-Glu-Val-Asp recognition sequence appeared to be conveniently compensated by the presence of the *t*Leu residue at the P2 position (Colantonio et al. 2008). Therefore, Z-*t*Leu-Asp-H appears as a promising candidate for the developing of pharmaceuticals to be used in modulating human caspase-3 activity.

Here, the role of the P2 *N*-capping group of the Z-*t*Leu-Asp-H di-peptidyl aldehyde on caspase-3 inhibition is reported. The *N*-carbobenzoxy moiety of Z-*t*Leu-Asp-H has been replaced with the acetyl, 2-chloro-benzyloxycarbonyl, and phenoxymethylcarbonyl (Fomc) groups (compounds **11**, **12**, and **13**, respectively, in Fig. 1). Moreover, *N*-acetyl- and *N*-benzyloxycarbonyl tri-peptidyl aldehyde caspase-3 inhibitors containing Asp at P1, *t*Leu or Leu at P2, and *t*Leu at P3 (compounds **27**–**29** in Fig. 1) have been synthesized. These new di- and tri-peptidyl aldehydes inhibit caspase-3 in vitro with K_i° values ranging between 6.5 (± 0.82) $\times\ 10^{-9}$ and 1.1 (± 0.04) $\times\ 10^{-7}$ M. Moreover, the most effective caspase-3 inhibitor Ac-*t*Leu-Asp-H (**11**) impairs apoptosis in human DLD-1 colon adenocarcinoma cells.

A computational modeling study has been also performed to elucidate the structural bases of caspase-3 inhibitor recognition, and to build a reliable model to be used in next generation inhibitor design. The computational study has been carried out exploiting a structure-based approach. The availability of caspase-3 crystallographic data, in fact, allowed us to apply docking calculations to simulate the binding between the studied peptides and the macromolecular target. Moreover, to validate the obtained binding mode and have a more accurate depiction of the recognition process, the MM-GBSA post-docking refinement method was applied to calculate the binding energies.

The presence of the *t*Leu residue in our inhibitors is not meaningless from the pharmacokinetic point of view, since peptides containing this sterically demanding amino acid have been shown to resist to both degradation by peptidases

and radical formation in vivo (Clements et al. 2001; Croft et al. 2003). Furthermore, to overcome the scarce membrane permeability of the current full-length inhibitors, the well-established strategy of truncation to tri- or even dipeptide scaffolds has been performed here, leading, through molecular mass reduction and removal of P4 carboxylate group, to a more favorable balance of hydrophilic/lipophilic properties in terms of bioavailability.

Materials

Human caspase-3, bovine serum albumin (BSA), trypsin, leupeptin, DMSO, DTT, sodium dodecyl sulfate (SDS), E2, L-glutamine, gentamicin, penicillin, staurosporine, tris (hydroxymethyl) aminomethane (Tris), phenylmethylsulfonyl fluoride (PMSF), RPMI-640, and fetal calf serum were purchased from Sigma–Aldrich (St. Louis, MO, USA). Bradford Protein Assay was obtained from BIO-RAD Laboratories (Hercules, CA, USA). The monoclonal anti-PARP and anti-tubulin antibodies were obtained from Santa Cruz Biotechnology (Santa Cruz, CA, USA). The ECL reagent for Western blot was obtained from Amersham Bioscience (Uppsala, Sweden). Amino acids and their derivatives were purchased from Sigma–Aldrich and Bachem. Analytical or reagent grade products were used without further purification.

Methods

Caspase-3 inhibitor synthesis

Peptides **11-13**, **27–29** were synthesized in satisfactory to good yields by adopting standard solution techniques (Bodanszky 1984), as reported in Fig. 1. The key compound H-Asp(O*t*Bu)-Sc (1) was synthesized according to literature (Graybill et al. 1994) and used for the subsequent *C*-to-*N* elongation steps. (*S*)-*tert*-leucine was routinely reacted with the appropriate acylating group to afford amino acid *N*-derivatives **2–4** and **15**, **20**. In details, protected dipeptides **5–7** and **16**, **17** were synthesized by EDAC/HOBt-mediated condensation of synton **1** with *N*-acylated *t*Leu (**2–4**, **15**) or Leu (**14**) derivatives. Dipeptides **16** and **17** were treated with equimolar 1,8-diazabicyclo (5.4.0) undec-7-ene (DBU) for Fmoc removal (Calcagni et al. 1999). *N*-deprotected semicarbazones **18** and **19** were coupled under standard conditions with the appropriate *t*Leu derivative Ac-*t*Leu-OH (2) or Z-*t*Leu-OH (**20**) to give tripeptides **21** and **22** (both from **18**), and **23** (from **19**). Fully protected intermediates **5–7** and **21–23** were subjected to acidolytic removal of the *O*-*t*Bu Asp side chain protection. Subsequent hydrolysis of the semicarbazone group with a mixture of MeOH/AcOH/37 % aq. HCHO generated the corresponding free aldehydes **11–13** and **27–29**, which were isolated in the tautomeric form of cyclic hemiacetals, as evidenced by CD_3OD NMR spectral data. Since final compounds were found unstable to reversed phase HPLC, they were purified to homogeneity by preparative layer chromatography and fully characterized by NMR spectroscopy. Details on experimental procedures are given in electronic Supplementary Material.

Caspase-3 inhibition in vitro

Caspase-3 catalyzed hydrolysis of Ac-Asp-Glu-Val-Asp-AMC, in the absence and presence of inhibitors, was followed spectrofluorimetrically at pH 7.4 (2.0×10^{-2} M phosphate buffer) and 25 °C (Barrett 1980; Garcia-Calvo et al. 1999; Ascenzi et al. 2006; Colantonio et al. 2008). Fluorescence (380 nm excitation wavelength, and 460 nm emission wavelength) was measured continuously over 10 min using a Jasco FP-6,500 fluorimeter (Jasco Corporation, Tokyo, Japan). Under all the experimental conditions, the fluorescence change (i.e., AMC release) was linear over the assay time (10 min). The amount of Ac-Asp-Glu-Val-Asp-AMC hydrolyzed by caspase-3 (i.e., of AMC) was calibrated letting the enzymatic reaction go to completion and measuring the amplitude of the signal at time ∞. The substrate and inhibitor stock solutions were prepared by dissolving Ac-Asp-Glu-Val-Asp-AMC and the inhibitors in DMSO (1.0×10^{-2} and 1.0×10^{-4} M, respectively). In the enzyme assay, the caspase-3 concentration was 7.0×10^{-10} M, the DTT concentration was 1.0×10^{-3} M, the Ac-Asp-Glu-Val-Asp-AMC concentration ranged between 5.0×10^{-9} and 5.0×10^{-5} M, and the inhibitor concentration ranged between 1.0×10^{-9} and 5.0×10^{-6} M.

Values of the intrinsic (i.e., v_i°, K_m°, and k_{cat}°) and apparent (i.e., v_i^{app}, K_m^{app}, and k_{cat}^{app}) catalytic parameters for caspase-3-catalyzed hydrolysis of Ac-Asp-Glu-Val-Asp-AMC were obtained in the absence and presence of **11–13** and **27–29** from the dependence of the initial velocity (i.e., v_i) on the substrate concentration (i.e., [S]), according to Eq. 1 (Michaelis and Menten 1913):

$$v_i = k_{cat} \times \frac{[S]}{(K_m + [S])} \quad (1)$$

Values of the apparent inhibition constant (i.e., K_i^{app}) for inhibitor binding to caspase-3 were obtained from the dependence of v_i^{app} on the inhibitor concentration (i.e., [I]) at fixed (Ac-Asp-Glu-Val-Asp-AMC), according to Eq. 2 (Ascenzi et al. 1987; Colantonio et al. 2008):

$$v_i^{app} = \frac{(v_i^\circ \times [I])}{(K_i^{app} + [I])} \quad (2)$$

Values of the intrinsic inhibition constant (i.e., K_i°) for inhibitor binding to caspase-3 were obtained from the dependence of K_i^{app} on the substrate concentration (i.e., [S]), according to Eq. 3 (Ascenzi et al. 1987; Colantonio et al. 2008):

$$K_i^\circ = K_i^{app} \times \left(1 + \frac{[S]}{K_m^\circ}\right) \quad (3)$$

Data are the mean ± standard deviation of at least three different experiments.

Caspase-3 inhibition in whole cells

Human DLD-1 colon adenocarcinoma cells were routinely grown in air containing 5 % CO_2 in modified phenol red-free RPMI-1,640 medium, containing 10 % (v/v) charcoal-stripped fetal calf serum, L-glutamine (2.0×10^{-3} M), gentamicin (0.1 mg/mL), and penicillin (100 U/mL). Cells were grown to ~70 % confluence and then treated with either the vehicle (DMSO 1 % v/v) or staurosporine (1.0×10^{-6} M) or E2 (1.0×10^{-8} M) in the absence and presence of **11** (final concentration ranging between 6.5×10^{-10} and 6.5×10^{-8} M). After treatments, cells were lysed and solubilized [in 1.25×10^{-1} M Tris, pH 6.8, containing 10 % (w/v) SDS, 1.0×10^{-3} M PMSF, and 5.0 μg/mL leupeptin] and finally boiled for 2 min. Total proteins were quantified using the Bradford Protein Assay. Solubilized proteins (20 μg) were electrophoretically resolved by 10 % SDS-PAGE (100 V, 1 h, 24 °C) and then transferred to nitrocellulose (30 V, overnight, 4 °C). The nitrocellulose membrane was treated with 3 % (w/v) BSA in 1.38×10^{-1} M NaCl, 2.5×10^{-2} M Tris buffer, pH 8.0, at 24 °C for 1 h and then probed overnight at 4 °C with anti-PARP antibody (1 μg/mL). The nitrocellulose membrane was stripped by Restore Western Blot Stripping Buffer (Pierce Chemical Company, Rockford, IL, USA) for 10 min at room temperature and then probed with anti-tubulin antibody. Antibody reaction was visualized with the ECL substrate for Western blot. All experiments were performed in 6-well plates loading 150,000 cells/well. At the end of each experiment, the cells were counted again and 200,000 ± 10,256 cells were present in each well.

The densitometric analyses were performed by ImageJ software for Windows. Statistical analysis was performed using Student's *t* test with the GraphPad INSTAT3 software system for Windows. In all cases, probability (*p*) values below 0.05 were considered significant. Data are the mean ± standard deviation of four different experiments carried out in duplicate.

Molecular modeling

All compounds were manually built in Maestro version 9.3.5 (Schrodinger), exploiting the Built facility. Ligands were reported in the hemiacetalic form, cyclized with Asp carboxylate as R and S enantiomers, and in alcoholic reduced form suitable for the docking calculations (see below). All structures were minimized to a derivative convergence of 0.001 $kJÅ^{-1}mol^{-1}$, using the Truncated Newton Conjugate Gradient (TNCG) minimization algorithm, the OPLS2005 force field, and the GB/SA water solvation model implemented in MacroModel version 9.9 (Schrodinger). Conformational searches, applying the Mixed torsional/Low-mode sampling and the automatic setup protocol, were carried out on all minimized ligand structures to obtain the global minimum geometry of each molecule, which was then used as the starting conformation for docking calculations with Glide version 5.8 (Schrödinger Suite 2012; Halgren et al. 2004; Friesner et al. 2004).

The three-dimensional structures of caspase-3 were downloaded from the Brookhaven Protein Data Bank (PDB ID: 2DKO, 2XYG, 1RHU, and 1RHQ). These models were submitted to the Protein Preparation routine in Maestro that allows fixing of receptor structures, eliminating water molecules and possible ligands, setting bond orders, adding hydrogen atoms, and computing the residues protonation state. To optimize the hydrogen bond network, His tautomers and ionization states were predicted, 180° rotations of the terminal χ angle of Asn, Gln, and His residues were assigned, and hydroxyl and thiol hydrogen atoms were sampled. For each structure, a brief relaxation was performed using an all-atom constrained minimization carried out with the Impact Refinement module version 5.8 (Schrödinger Suite 2012) and the OPLS-2,005 force field to reduce steric clashes that may exist in the original PDB structures. The minimization was terminated when the energy converged or the root mean square deviation (RMSD) reached a maximum cutoff of 0.30 Å. To carry out docking calculations with Glide, that is not able to perform covalent ligand docking, the catalytic Cys163 residue was mutated into Ala to allow ligands to properly accommodate in the binding site without steric clashes with the Cys163 side chain. To guarantee the correct positioning of the inhibitor, a constraint was imposed whereby just ligand poses placing the "hemiacetalic" carbon in the same position of the crystallographic ligand (at almost 3 Å from the Cα of Cys163), were saved.

Glide energy grid for each enzyme structure was generated using the crystallographic ligand as the center of the grid. The size of the box was determined automatically on the basis of the ligand dimensions. The global minimum geometry of ligands was submitted to docking calculations in the previously prepared proteins. The van der Waals radii for non-polar ligand atoms were scaled by a factor of 0.8, thereby decreasing penalties for close contacts. A first docking run was carried out applying the standard precision (SP) settings of Glide. Ten poses were retrieved and

re-submitted to the extra precision (XP) docking routine (Friesner et al. 2006), saving one pose.

The described docking protocol was applied to the initial cross-docking of selected crystal complexes as well as to peptidyl aldehydes under study. For the evaluation of the cross-docking results, the ligand poses were compared to the crystallographic ones, to select the caspase-3 3D-structure able to correctly predict the X-ray ligand binding mode. The caspase-3 three-dimensional structure with PDB ID 2DKO provided the best results in cross-docking and was used in the docking calculations (SP and XP) on compounds under study.

The best ranking pose for each ligand was considered for the following MM-GBSA analysis. The simulation was performed on the receptor-ligand complex obtained from XP molecular docking, that was minimized using the local optimization feature in Prime, whereas the energies of the complex were calculated with the OPLS-2005 force field and the parameterized solvation model (Zhu et al. 2006, 2007). During the simulation process, the ligand strain energy was also considered. A user-defined scoring function was generated from the energy term calculated by Prime MM-GBSA using the Multiple Linear Regression method in Strike (Schrödinger Suite 2012), allowing the automatic selection of the optimal subset. The leave one out (LOO) cross-validation analysis was used to estimate the prediction ability of the model.

Molecular graphic images were produced by using Pymol (PyMOL 2009). All calculations were performed on a DELL T5500 workstation, equipped with two Intel® Xeon® E5630 2.53 GHz processors.

Results and discussion

Caspase-3 inhibition in vitro

In the absence and presence of dipeptides **11–13** and tripeptides **27–29** caspase-3 catalyzed hydrolysis of Ac-Asp-Glu-Val-Asp-AMC follows simple Michaelis–Menten kinetics. Values of K_m° and k_{cat}° here obtained [4.8 (±0.4) × 10^{-6} M and 9.8 ± 1.3 s^{-1}, respectively] agree well with those reported in the literature (Garcia-Calvo et al. 1999; Ascenzi et al. 2006; Colantonio et al. 2008).

Compounds **11–13** and **27–29** inhibit caspase-3-catalyzed hydrolysis of Ac-Asp-Glu-Val-Asp-AMC competitively. Indeed, values of K_m^{app} increase with the inhibitor concentration (data not shown). Moreover, the value of $k_{cat}^\circ = k_{cat}^{app} = 9.8 \pm 1.3\ s^{-1}$ is unaffected by the inhibitor concentration (data not shown). Furthermore, values of K_i^{app} increase with the Ac-Asp-Glu-Val-Asp-AMC concentration (Fig. 2a, b; Fig. S1 of electronic Supplementary Material). Data analysis according to Eq. (3) allowed determining values of K_i° ranging between 6.5 (±0.82) × 10^{-9} and 1.1 (±0.04) × 10^{-7} M (see Table 1). Remarkably, experimentally determined and predicted (see below) values of K_i° match very well each other (see Table 1).

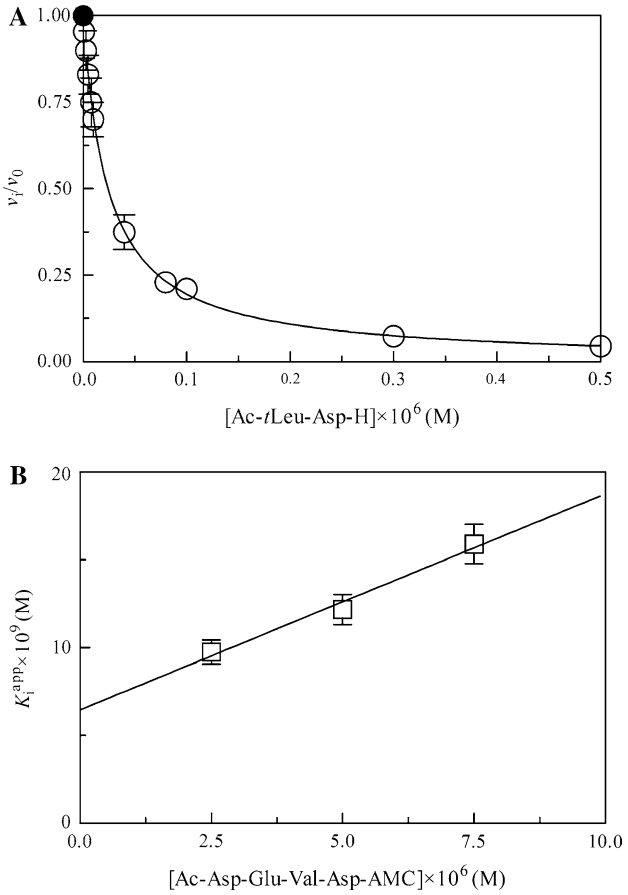

Fig. 2 Inhibition of caspase-3 catalyzed hydrolysis of Ac-Asp-Glu-Val-Asp-AMC by Ac-*t*Leu-Asp-H (**11**), at pH 7.4 and 25 °C. **a** Dependence of v_i^{app}/v_i° on the Ac-*t*Leu-Asp-H concentration. The filled circle on the ordinate indicates the v_i^{app}/v_i° ratio in the absence of **11**. The analysis of data according to Eq. (2) allowed determining the value of K_i^{app} = 1.2 (±0.12) × 10^{-8} M. The substrate concentration was 5.0 × 10^{-6} M. **b** Dependence of K_i^{app} on the Ac-Asp-Glu-Val-Glu-AMC concentration. The analysis of data according to Eq. (3) allowed determining the value of K_i° = 6.5 (±0.8) × 10^{-9} M. Where not shown, the standard deviation is smaller than the symbol. For details, see the text

The analysis of data given in Table 1 for human caspase-3 inhibition by all the available di-, tri-, and tetrapeptidyl aldehydes allows the following considerations. Ac-Asp-Glu-Val-Asp-H is the prototypical inhibitor of human caspase-3, corresponding to the recognition sequence of the cleavage site of PARP (K_i° = 2.3 × 10^{-10} M; pH 7.5 and 25.0 °C) (Rotonda et al. 1996; Mittl et al. 1997; Talanian et al. 1997; Thornberry et al. 1997; Garcia-Calvo et al. 1998; Wei et al. 2000; Chatterjee et al. 2004; Kanthasamy et al. 2006; Howley and Fearnhead 2008; Fang et al. 2009; Rohn 2010). The enzyme/inhibitor affinity is affected by amino

Table 1 Values of $K_i°$ for human caspase-3 inhibition by di-, tri-, and tetra-peptidyl aldehydes

Inhibitor consensus sequence					$K_i°$ or IC_{50} (M)	
P5	P4	P3	P2	P1	Experimental	Predicted
Ac	Asp	Glu	Val	Asp-H[a]	$K_i° = 2.3 \times 10^{-10}$	$K_i° = 2.6 \times 10^{-10}$
Ac	Ala	Glu	Val	Asp-H[a]	$K_i° = 4.2 \times 10^{-8}$	$K_i° = 6.7 \times 10^{-8}$
Ac	Ile	Glu	Thr	Asp-H[a]	$K_i° = 2.0 \times 10^{-7}$	$K_i° = 1.4 \times 10^{-7}$
Ac	Trp	Glu	His	Asp-H[a]	$K_i° = 2.0 \times 10^{-6}$	$K_i° = 2.9 \times 10^{-6}$
Ac	Tyr	Val	Ala	Asp-H[b]	$K_i° = 1.2 \times 10^{-5}$	$K_i° = 7.0 \times 10^{-6}$
Ac	Ala	Pro	*n*Leu	Asp-H[c]	$K_i° = 4.5 \times 10^{-5}$	$K_i° = 3.2 \times 10^{-5}$
Ac	Asp	Met	Gln	Asp-H[d]	$K_i° = 1.2\ (\pm 0.74) \times 10^{-8}$	$K_i° = 1.9 \times 10^{-8}$
	Z	Glu	Leu	Asp-H[e]	$IC_{50} = 2.3 \times 10^{-9}$	
	Z	*t*Leu	Val	Asp-H[f]	$K_i° = 1.8\ (\pm 0.1) \times 10^{-8}$	$K_i° = 1.2 \times 10^{-8}$
	Z	Val	*t*Leu	Asp-H[f]	$K_i° = 1.1\ (\pm 0.1) \times 10^{-7}$	$K_i° = 1.5 \times 10^{-7}$
	Z	Phe	Leu	Asp-H[e]	$IC_{50} = 1.4 \times 10^{-7}$	
	Z	Pro	*n*Leu	Asp-H[c]	$K_i° = 2.2 \times 10^{-5}$	$K_i° = 2.3 \times 10^{-5}$
	Ac	*t*Leu	*t*Leu	Asp-H[g]	$K_i° = 1.6\ (\pm 0.1) \times 10^{-8}$	$K_i° = 7.2 \times 10^{-9}$
	Ac	*t*Leu	Leu	Asp-H[g]	$K_i° = 1.1\ (\pm 0.008) \times 10^{-8}$	$K_i° = 1.7 \times 10^{-8}$
	Z	*t*Leu	Leu	Asp-H[g]	$K_i° = 1.1\ (\pm 0.04) \times 10^{-7}$	$K_i° = 4.0 \times 10^{-7}$
		Z	*t*Leu	Asp-H[f]	$K_i° = 3.6\ (\pm 0.4) \times 10^{-9}$	$K_i° = 4.6 \times 10^{-9}$
		Z	Val	Asp-H[e]	$IC_{50} = 1.8 \times 10^{-6}$	
		Z	Leu	Asp-H[e]	$IC_{50} = 3.5 \times 10^{-6}$	
		Ac	*t*Leu	Asp-H[g]	$K_i° = 6.5\ (\pm 0.82) \times 10^{-9}$	$K_i° = 8.1 \times 10^{-9}$
		2-Cl-Z	*t*Leu	Asp-H[g]	$K_i° = 2.3\ (\pm 0.07) \times 10^{-8}$	$K_i° = 9.8 \times 10^{-9}$
		Fomc	*t*Leu	Asp-H[g]	$K_i° = 6.3\ (\pm 0.2) \times 10^{-8}$	$K_i° = 5.5 \times 10^{-8}$

[a] pH 7.5 and 22.0 °C. The error values were never >10 %. From (Garcia-Calvo et al. 1998)

[b] pH 7.5 and 25.0 °C. The error values were not reported. From (Mittl et al. 1997)

[c] pH 7.5 and 25.0 °C. The error values were not reported. From (Kisselef et al. 2003)

[d] pH 7.5 and 25.0 °C. From (Fang et al. 2006)

[e] pH 7.5 and 25.0 °C. From (Linton et al. 2002)

[f] pH 7.4 and 25.0 °C. From (Colantonio et al. 2008)

[g] pH 7.4 and 25.0 °C. Present study

acid residue substitution(s) at positions P4, P3, and P2, the P1 position being always occupied by Asp-H; values of K_i^0 span over five orders of magnitude [see (Mittl et al. 1997; Garcia-Calvo et al. 1998; Linton et al. 2002; Kisselev et al. 2003; Chatterjee et al. 2004; Fang et al. 2006; Colantonio et al. 2008) and the present study]. The presence of the Ala residue at the P4 position reduces the Ac-Ala-Glu-Leu-Asp-H affinity for human caspase-3 by two orders of magnitude. The combined substitution of amino acid residues at positions P4, P3, and P2 decreases the affinity of tetra-peptidyl aldehydes for caspase-3 up to five orders of magnitude. The truncation of the P4 residue, the substitution of the *N*-terminal acetyl blocking group with the carbobenzoxy group, and the substitution of Val at position P2 with Leu reduces the inhibitor affinity for human caspase-3. Moreover, the truncation of the P4 residue and the concomitant amino acid residue substitutions at the P3 and P2 positions affect significantly the affinity of tri-peptidyl aldehydes for human caspase-3, $K_i°$ values increasing from $1.1\ (\pm 0.008) \times 10^{-8}$–$2.2 \times 10^{-5}$ M. Remarkably, the presence of the Pro and *n*Leu residues at positions P3 and P2, respectively, reduces dramatically the affinity of Ac-Ala-Pro-*n*Leu-Asp-H and Z-Pro-nLeu-Asp-H for human caspase-3 ($K_i° = 4.5 \times 10^{-5}$ and 2.2×10^{-5} M, respectively). Finally, the presence of the non-proteinogenic *t*Leu residue at position P2 facilitates di-peptidyl aldehyde recognition by human caspase-3, the most favorable inhibitors being Z-*t*Leu-Asp-H and Ac-*t*Leu-Asp-H (**11**) [$K_i° = 3.6\ (\pm 0.4) \times 10^{-9}$ and $6.5\ (\pm 0.82) \times 10^{-9}$ M, respectively]. The presence of Leu and Val residues at the P2 position decreases the affinity of di-peptidyl aldehyde inhibitors for human caspase-3 by about three orders of magnitude.

Caspase-3 inhibition in whole cells

Several studies have demonstrated that E2 is a pro-apoptotic hormone in the presence of the estrogen receptor β subtype modulating the cell cycle machinery, suppressing DNA synthesis, and inducing caspase-dependent apoptosis (Caiazza et al. 2007; Galluzzo et al. 2007; Bolli et al. 2010; Bulzomi et al. 2012). 24 h incubation of DLD-1 colon cancer cells with 1.0×10^{-8} M E2 induces the caspase-3 pro-form activation, which results in the cleavage of the 116-kDa DNA repair enzyme PARP. Western blot analysis confirms that treatment of DLD-1 cells with E2 results in the conversion of PARP into the inactive 85-kDa fragment. Similar result has been obtained stimulating cells with staurosporine (1.0×10^{-6} M), a well-known inducer of apoptosis (Jiang et al. 2013; Son et al. 2014). DLD-1 cells pre-treatment with Ac-*t*Leu-Asp-H (**11**) (6.5×10^{-10}–6.5×10^{-8} M) completely prevented E2-induced PARP cleavage (Fig. 3a, b). To evaluate the DLD-1 cell death upon treatment with **11**,

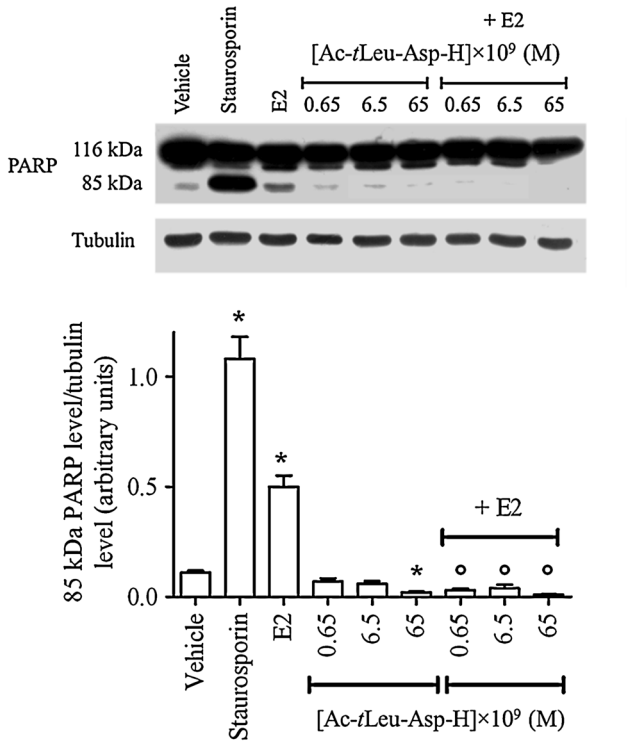

Fig. 3 Western blot (**a**) and densitometric analysis of PARP (**b**) isolated by DLD-1 cells stimulated for 24 h with vehicle or staurosporine (1.0×10^{-6} M), 17β-estradiol (E2; 1.0×10^{-8} M) in the absence and presence of Ac-*t*Leu-Asp-H (**11**). Data are the mean ± standard deviation of four different experiments carried out in duplicate. $P < 0.001$, calculated with Student's *t* test, was compared with *asterisk* non-stimulated control values (vehicle) or with *degree* E2-treated values. For details, see the text

DLD-1 cells were counted before and after each experiment. All experiments were performed in 6-well plates loading 150,000 cells/well. At the end of each experiment, the cells were counted again and 200,000 ± 10,256 cells were present in each well. Therefore, treatment with **11** at inhibitory concentrations effective in vitro (6.5×10^{-10}, 6.5×10^{-9} and 6.5×10^{-8} M; see Fig. 3 for comparison) did not exert any cytotoxic effects in adenocarcinoma DLD-1 cells at the time considered.

These results indicate that **11** inhibits the caspase-3 activity in whole cells.

Molecular modeling

Inhibitor docking to caspase-3 and MM-GBSA

To rationalize the activity data, the binding mode of the new caspase-3 inhibitors was analyzed through docking studies. To obtain meaningful results, eight more peptidyl aldehydes with reported K_i toward caspase-3 were included in the model (Table 1).

Docking calculations were performed using the standard precision (SP) and the extra precision (XP) docking protocol. The XP scoring function contains a number of additional terms beyond those present in GlideScore, that result in a better prediction of the docking poses and a closer correlation with the experimental results. However, it is well known that docking scores hardly correlate with experimental binding affinities. To improve the accuracy of the binding energy prediction, the Prime/MM-GBSA method was used to refine the docked pose of each ligand. The MM-GBSA method applies the following equation:

$$\Delta G_{\text{bind}} = \Delta E_{\text{MM}} + \Delta G_{\text{solv}} + \Delta G_{\text{SA}} \quad (4)$$

where ΔE_{MM} is the difference in the minimized energies between the complex and the sum of the energies of the apo-protein and the ligand, ΔG_{solv} is the difference in the GBSA solvation energy of the complex and the sum of the solvation energies for the apo-protein and the ligand, and ΔGSA is the difference in surface area energies for the complex and the sum of the surface area energies for the apo-protein and the ligand.

Energy parameters, calculated through this approach, were used to generate a user-defined scoring function that, weighting the single energy contribution, can provide a better interpretation of forces driving the binding process. The developed scoring function (5):

$$\begin{aligned} \text{p}K_i = &-0.332\ (\pm 0.065) - 0.038\ (\pm 0.005) \\ &\times \text{Complex vdW} - 0.234\ (\pm 0.016) \\ &\times \text{Ligand Covalent} - 0.013\ (\pm 0.003) \\ &\times \text{Ligand Solvation GB} - 0.113\ (\pm 0.025) \\ &\times \text{Ligand Strain Energy} - 0.057\ (\pm 0.017) \\ &\times \text{Receptor Strain Covalent} \end{aligned} \quad (5)$$

was able to provide a significant correlation between the predicted and the experimental K_i values (Table 1), with solid statistical parameters ($R^2 = 0.97$, SD = 0.31, $Q^2 = 0.94$, $F = 64.4$, and $P = 9.1 \times 10^{-8}$), that underpin the reliability of the model.

The analysis of the scoring function highlights the contribution of van der Waals interactions to the binding energy (Complex VdW), especially due to the interactions occurring in the S2 site. Besides this expected factor, also the conformational and solvation energies of the ligands (Ligand Covalent, Ligand Strain Energy and Ligand Solv GB), i.e., the energy spent by the ligand moving from the solvent to the binding site, play a relevant role, confirming what suggested by conformational search results (See electronic Supplementary Material for a more detailed explanation of the scoring function terms).

Poses obtained from MM-GBSA show that all ligands adopt a very similar binding mode with the following conserved interactions: one H-bond between the Asp

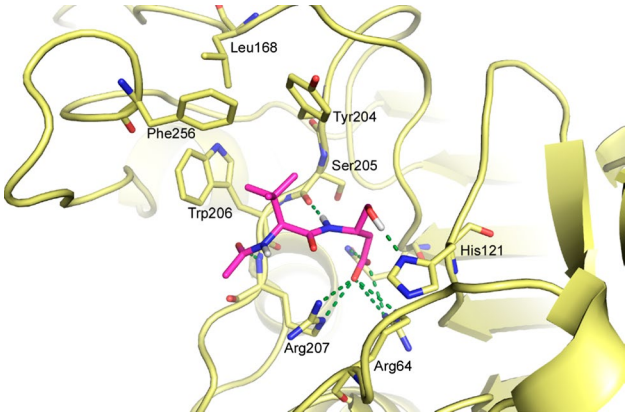

Fig. 4 Structure of the human caspase-3 in complex with Ac-*t*Leu-Asp-H (**11**) as resulting from docking calculations. Caspase-3 structure is depicted as a pale-yellow cartoon, while **11** is represented with magenta C-atoms. Docked ligand and most relevant residues are shown as sticks. H-bonds between the ligand and caspase-3 residues are shown as green dashed lines

hemiacetalic OH group and the His121 δN; one H-bond network between the Asp carboxylate group and the Arg64, Arg207, and Gln161 residues; one H-bond between the Asp NH and the Ser205 CO; and one H-bond between the Z/Ac CO and the Arg207 backbone NH. The side chain of the P2 residue establishes several hydrophobic interactions with the Phe256, Trp206, Tyr204, and Leu168 residues, while the P3 hydrophobic side chain (when present) partially occupies the S3 site arranging favorable contacts with the Arg207 alkyl chain (Fig. 4). Differences can be observed for the positioning of the *N*-terminal substituent. Moreover, the introduction of a bulky hydrophobic group does not provide an activity enhancement in most of the cases.

Focusing on di-peptidyl aldehydes, the substitution of the carbobenzoxy (lead compound) with an acetyl group (as in **11**) was shown to have no significant impact on activity. In fact, **11** binds very efficiently to the caspase-3 active site owning the structural determinants for the activity, as confirmed by calculating the ligand efficiency (LE) (Hopkins et al. 2004) (Table S2 in Supplementary Material). LE accounts for the average energetic contribution provided by each heavy atom to the global binding energy:

$$\mathrm{LE} = -\frac{\Delta G}{N_{\text{non-H atoms}}} \tag{6}$$

As Z-*t*Leu-Asp-H and **11** have the same binding mode, most likely the binding energy difference between these ligands ($\Delta\Delta G_{\text{bind}} = 0.3$ kcal) can be attributed to the benzyloxy group (7 atoms); therefore, this group affords an average energy contribution per atom equal to a negligible value of 0.04 kcal. The binding poses analysis confirms this observation; in fact, the benzyloxy group of the lead compound is not able to find a specific interaction in the active site and bends to find some contacts with the Trp206, Phe256, and *t*Leu side chain, similarly to **12** that does not find interactions for the Cl substituent that remains solvent exposed. On the other hand, the phenoxymethyl group of **13** occupies the binding cleft in an extended conformation, with no specific interactions of the aromatic ring.

Ligand elongation with an additional residue does not improve the inhibition effect. The energetic gain provided by tri-peptides is counterbalanced by the conformational effort; in fact, the ligand strain energy calculated for tri-peptide docked poses is generally high. Similarly to di-peptides, the benzyloxycarbonyl *N*-terminal group does not participate to any specific interaction and does not improve the activity with respect to acetyl derivatives. However, Z-*t*Leu-Val-Asp-H seems to behave differently; in fact, the scaffold binding mode is conserved (see above), but the scoring function parameters indicate that this inhibitor forms more favorable van der Waals contacts in complex with caspase-3 and a much lower ligand strain; therefore, it may be concluded that the combination of *t*Leu and Val at P3 and P2, respectively, allows the molecule to bind in a low-energy conformation.

Role of the tLeu residue in P2

The efficiency of the *t*Leu residue at the P2 position has been disclosed previously (Colantonio et al. 2008) and confirmed in the present study. To better understand the reason of this unexpected high affinity, we compared the inhibitor Z-*t*Leu-Asp-H ($IC_{50} = 7.3 \times 10^{-9}$ M) to previously reported inhibitors Z-Val-Asp-H and Z-Leu-Asp-H ($IC_{50} = 1.8 \times 10^{-6}$ and $IC_{50} = 3.5 \times 10^{-6}$ M, respectively) (Linton et al. 2002). These ligands were selected because Val was predicted as the preferred residue in S2 (Yoshimori et al. 2004) and Leu is the natural isomer of *t*Leu. These dipeptides were submitted to docking and post-docking refinement highlighting a very similar binding geometry. Consequently, to better understand the different affinity, the single energetic contributions were analyzed. Quite surprisingly, the *t*Leu residue does not provide an improvement of van der Waals interactions, in fact one methyl group of the *t*Leu side chain results solvent exposed, but it has a much lower conformational energy; therefore, it binds efficiently spending less energy than other dipeptides. This result is in line with the scoring function (5) and confirms the role of hydrophobic contacts and of the ligand strain energy in determining the activity of this class of inhibitors.

Conclusion

In the present work, we disclose a panel of new di- and tri-peptidyl aldehydes as nanomolar competitive inhibitors of

human caspase-3. Regarding the inhibitory activity of peptides on caspase-3, the current study presents an encouraging correlation between experimental data and computational results (see Table 1). Docking calculations and post-docking refinement with the MM-GBSA method provide a rationale to enzyme inhibition, highlighting as the predicted binding mode and, therefore, the enzyme/inhibitor interactions are very conserved among di- and tri-peptidyl aldehydes. The driving force for inhibitors binding to caspase-3 is strongly related to the conformational energy spent by the ligand to accommodate in the binding site.

Consistent with our previous data (Colantonio et al. 2008), further evidence is added here that the enzyme activity may be drastically inhibited by peptidyl aldehydes consisting of only two amino acids, confirming the *t*Leu-Asp as the most effective minimal recognition motif for caspase-3. Considering the near absolute requirement for Asp at the P1 position, the P2 specificity of caspase-3 for the non-proteinogenic amino acid *t*Leu is precisely defined, opening new perspectives in the search of new anti-apoptotic drugs with more favorable pharmacokinetic properties. Calculations suggest that the *t*Leu residue at P2 position favorably contributes to the ligand adaptation to the enzyme active site by lowering the conformational strain paid during the binding process.

To investigate further stereoelectronic and conformational contributes expected to be beneficial to affinity and inhibiting potency, an *N*-capping refinement at the *N*-terminus of the dipeptide sequence has been performed, leading to identification of the acetyl group as the minimal effective probe. With the exception of the already reported *N*-benzyloxycarbonyl derivative Z-*t*Leu-Asp-H, the addition of groups larger than acetyl at the *N*-terminus does not increase the inhibitory effect of the resulting peptides. The analysis of the computed binding modes of the ligands into the active site indicates that the bulky *N*-acylating portions do not sensibly contribute to binding affinity, since they do not find any specific contacts in the binding cleft.

A scrutiny of tri-peptidyl aldehydes allows a distinction between intermediate and high affinity peptide inhibitors. In the P3 *t*Leu-based series, the shift from *N*-acetyl to *N*-benzyloxycarbonyl moieties reduces the affinity for caspase-3 by one order of magnitude, except for Z-*t*Leu-Val-Asp-H. Computational evidence endorses the role of conformational and hydrophobic binding energies for this entry. Interestingly, a good inhibitory activity is maintained by the tripeptide **29** containing the bulky *t*Leu–*t*Leu motif, which is expected to influence the conformational preferences of the molecule (Formaggio et al. 2005).

Finally, the most active inhibitor **11** has a marked anti-apoptotic effect in whole cells efficiently preventing the ability of the hormone estrogen to induce the caspase-3-mediated PARP cleavage in DLD-1 colon cancer cells. The capability of **11** to inhibit the apoptotic machinery suggests a good permeability of this compound throughout the plasma membrane of living cells opening meaningful opportunities for medical applications. In this context, the small molecule approach is confirmed here as a winning strategy in the rational design of potent caspase-3 peptide inhibitors to be used for cytoprotection. Future directions will include the optimization of pharmacokinetic and activity/selectivity profiles of our compounds to advance them to deliverable drugs.

Acknowledgments This study was supported by grants from Ministry of Education, University, and Research of Italy (University "Gabriele d'Annunzio", ex 60 % 2013 to G.L. and M.A., and University Roma Tre, CAL 2013 to P.A.).

Conflict of interest The authors declare that they have no conflict of interest.

Ethical standard The manuscript does not contain clinical studies or patient data.

References

Ascenzi P, Ascenzi MG, Amiconi G (1987) Enzyme competitive inhibition. Graphical determination of *K*i and presentation of data in comparative studies. Biochem Educ 15:134–135

Ascenzi P, Marino M, Menegatti E (2006) CO_2 impairs peroxynitrite-mediated inhibition of human caspase-3. Biochem Biophys Res Commun 349:367–371

Barrett AJ (1980) Fluorimetric assays for cathepsin B and cathepsin H with methylcoumarylamide substrates. Biochem J 187:909–912

Bergmann A, Steller H (2010) Apoptosis, stem cells, and tissue regeneration. Sci Signal 3:re8

Bodanszky M (1984) Principles of Peptide Synthesis. Springer-Verlag, Berlin. ISBN 3-540-12395-4

Bolli A, Bulzomi P, Galluzzo P, Acconcia F, Marino M (2010) Bisphenol A impairs estradiol-induced protective effects against DLD-1 colon cancer cell growth. IUBMB Life 62:684–687

Bulzomi P, Galluzzo P, Bolli A, Leone S, Acconcia F, Marino M (2012) The pro-apoptotic effect of quercetin in cancer cell lines requires ERβ-dependent signals. J Cell Physiol 227:1891–1898

Caiazza F, Galluzzo P, Lorenzetti S, Marino M (2007) 17β-estradiol induces ERβ up-regulation via p38/MAPK activation in colon cancer cells. Biochem Biophys Res Commun 359:102–107

Calcagni A, Lucente G, Luisi G, Pinnen F, Rossi D (1999) Novel glutathione analogues containing the dithiol and disulfide form of the Cys–Cys dyad. Amino Acids 17:257–265

Chatterjee PK, Todorovic Z, Sivarajah A, Mota-Filipe H, Brown PAJ, Stewart KN, Cuzzocrea S, Thiemermann C (2004) Differential effects of caspase inhibitors on the renal dysfunction and injury caused by ischemia-reperfusion of the rat kidney. Eur J Pharmacol 503:173–183

Chowdhury I, Tharakan B, Bhat GK (2008) Caspases—an update. Comp Biochem Physiol B Biochem Mol Biol 151:10–27

Clements JM, Beckett RP, Brown A, Catlin G, Lobell M, Palan S, Thomas W, Whittaker M, Wood S, Salama S, Baker PJ, Rodgers HF, Barynin V, Rice DW, Hunter MG (2001) Antibiotic activity and characterization of BB-3497, a novel peptide deformylase inhibitor. Antimicrob Agents Chemother 45:563–570

Colantonio P, Leboffe L, Bolli A, Marino M, Ascenzi P, Luisi G (2008) Human caspase-3 inhibition by Z-*t*Leu-Asp-H: *t*Leu(P2) counterbalances Asp(P4) and Glu(P3) specific inhibitor truncation. Biochem Biophys Res Commun 377:757–762

Croft AK, Easton CJ, Radom L (2003) Design of radical-resistant amino acid residues: a combined theoretical and experimental investigation. J Am Chem Soc 125:4119–4124

Fang B, Boross PI, Tozser J, Weber IT (2006) Structural and kinetic analysis of caspase-3 reveals role for S5 binding site in substrate recognition. J Mol Biol 360:654–666

Fang B, Fu G, Agniswamy J, Harrison RW, Weber IT (2009) Caspase-3 binds diverse P4 residues in peptides as revealed by crystallography and structural modeling. Apoptosis 14:741–752

Formaggio F, Baldini C, Moretto V, Crisma M, Kaptein B, Broxterman QB, Toniolo C (2005) Preferred conformations of peptides containing *tert*-leucine, a sterically demanding, lipophilic α-amino acid with a quaternary side-chain Cβ atom. Chemistry 11:2395–2404

Friesner RA, Banks JL, Murphy RB, Halgren TA, Klicic JJ, Mainz DT, Repasky MP, Knoll EH, Shaw DE, Shelley M, Perry JK, Francis P, Shenkin PS (2004) Glide: a new approach for rapid, accurate docking and scoring. 1. Method and assessment of docking accuracy. J Med Chem 47:1739–1749

Friesner RA, Murphy RB, Repasky MP, Frye LL, Greenwood JR, Halgren TA, Sanschagrin PC, Mainz DT (2006) Extra precision glide: docking and scoring incorporating a model of hydrophobic enclosure for protein-ligand complexes. J Med Chem 49:6177–6196

Galluzzo P, Caiazza F, Moreno S, Marino M (2007) Role of ERβ palmitoylation in the inhibition of human colon cancer cell proliferation. Endocr Relat Cancer 14:153–167

Ganesan R, Jelakovic S, Campbell AJ, Li ZZ, Asgian JL, Powers JC, Grütter MG (2006) Exploring the S4 and S1 prime subsite specificities in caspase-3 with aza-peptide epoxide inhibitors. Biochemistry 45:9059–9067

Garcia-Calvo M, Peterson EP, Leiting B, Ruel R, Nicholson DW, Thornberry NA (1998) Inhibition of human caspases by peptide-based and macromolecular inhibitors. J Biol Chem 273:32608–32613

Garcia-Calvo M, Peterson EP, Rasper DM, Vaillancourt JP, Zamboni R, Nicholson DW, Thornberry NA (1999) Purification and catalytic properties of human caspase family members. Cell Death Differ 6:362–369

Graybill TL, Dolle RE, Helaszek CT, Miller RE, Ator MA (1994) Preparation and evaluation of peptidic aspartyl hemiacetals as reversible inhibitors of interleukin-1β converting enzyme (ICE). Int J Pept Protein Res 44:173–182

Halgren TA, Murphy RB, Friesner RA, Beard HS, Frye LL, Pollard WT, Banks JL (2004) Glide: a new approach for rapid, accurate docking and scoring. 2. Enrichment factors in database screening. J Med Chem 47:1750–1759

Hopkins AL, Groom CR, Alex A (2004) Ligand efficiency: a useful metric for lead selection. Drug Discov Today 9:430–431

Howley B, Fearnhead HO (2008) Caspases as therapeutic targets. J Cell Mol Med 12:1502–1516

Jiang P, Wang J, Kang Z, Li D, Zhang D (2013) Porcine JAB1 significantly enhances apoptosis induced by staurosporine. Cell Death Dis 4:e823

Kanthasamy AG, Anantharam V, Zhang D, Latchoumycandane C, Jin H, Kaul S, Kanthasamy A (2006) A novel peptide inhibitor targeted to caspase-3 cleavage site of a proapoptotic kinase protein kinase C delta (PKCδ) protects against dopaminergic neuronal degeneration in Parkinson's disease models. Free Radic Biol Med 41:1578–1589

Kisselev AF, Garcia-Calvo M, Overkleeft HS, Peterson E, Pennington MW, Ploegh HL, Thornberry NA, Goldberg AL (2003) The caspase-like sites of proteasomes, their substrate specificity, new inhibitors and substrates, and allosteric interactions with the trypsin-like sites. J Biol Chem 278:35869–35877

Linton SD, Karanewsky DS, Ternansky RJ, Wu JC, Pham B, Kodandapani L, Smidt R, Diaz JL, Fritz LC, Tomaselli KJ (2002) Acyl dipeptides as reversible caspase inhibitors. Part 1: initial lead optimization. Bioorg Med Chem Lett 12:2969–2971

Michaelis L, Menten M (1913) Die Kinetik der Invertinwirkung. Biochem Z 49:333–369

Mittl PRE, di Marco S, Krebs JF, Bai X, Karanewsky DS, Priestle JP, Tomaselli KJ, Grütter MG (1997) Structure of recombinant human CPP32 in complex with the tetrapeptide acetyl-Asp-Val-Ala-Asp fluoromethyl ketone. J Biol Chem 272:6539–6547

Nedev HN, Klaiman G, LeBlanc A, Saragovi HU (2005) Synthesis and evaluation of novel dipeptidyl benzoyloxymethyl ketones as caspase inhibitors. Biochem Biophys Res Commun 336:397–400

PyMOL (TM), version 1.2r1, DeLano Scientific LLC (2009)

Rohn TT (2010) The role of caspases in Alzheimer's disease; potential novel therapeutic opportunities. Apoptosis 15:1403–1409

Rotonda J, Nicholson DW, Fazil KM, Gallant M, Gareau Y, Labelle M, Peterson EP, Rasper DM, Ruel R, Vaillancourt JP, Thornberry NA, Becker JW (1996) The three-dimensional structure of apopain/CPP32, a key mediator in apoptosis. Nat Struct Biol 3:619–625

Schrödinger Suite (2012) Maestro, version 9.3; MacroModel, version 9.9; Glide, version 5.8, Prime, version 3.1. Schrödinger LLC, New York

Son D, Na YR, Hwang ES, Seok SH (2014) Platelet-derived growth factor-C (PDGF-C) induces anti-apoptotic effects on macrophages through Akt and Bad phosphorylation. J Biol Chem 289:6225–6235

Talanian RV, Quinlan C, Trautz S, Hackett MC, Mankovich JA, Banach D, Ghayur T, Brady KD, Wong WW (1997) Substrate specificities of caspase family proteases. J Biol Chem 272:9677–9682

Thornberry NA (1998) Caspases: key mediators of apoptosis. Chem Biol 5:R97–R103

Thornberry NA, Rano TA, Peterson EP, Rasper DM, Timkey T, Garcia-Calvo M, Houtzager VM, Nordstrom PA, Roy S, Vaillancourt JP, Chapman KT, Nicholson DW (1997) A combinatorial approach defines specificities of members of the caspase family and granzyme B. Functional relationships established for key mediators of apoptosis. J Biol Chem 272:17907–17911

Wei Y, Fox T, Chambers SP, Sintchak J, Coll JT, Golec JM, Swenson L, Wilson KP, Charifson PS (2000) The structures of caspases-1, -3, -7 and -8 reveal the basis for substrate and inhibitor selectivity. Chem Biol 7:423–432

Yoshimori A, Takasawa R, Tanuma S (2004) A novel method for evaluation and screening of caspase inhibitory peptides by the amino acid positional fitness score. BMC Pharmacol 4:Art 7

Zhu K, Pincus DL, Zhao S, Friesner RA (2006) Long loop prediction using the protein local optimization program. Proteins (Struct Funct Bioinformat) 65:438–452

Zhu K, Shirts M, Friesner RA (2007) Improved methods for side chain and loop predictions via the protein local optimization program: variable dielectric model for implicitly improving the treatment of polarization effects. J Chem Theor Comput 3:2108–2119